Excerpt from the Proceedings of the 2011 COMSOL Conference in Boston

Calculating Opto-Mechanically Induced Surface Acoustic Waves in a SilicaWhispering Gallery Microresonator

John Zehnpfennig*
Photonics Research Center, United States Military Academy, West Point, NY, USA
*MADN-PRC, Bartlett Hall, Bldg. 753, Room B21, West Point, NY 10996. john.zehnpfennig@usma.edu

Abstract: Here we calculate using COMSOL opto-mechanically induced Surface Acoustic Waves upon a silica microresonator. Using conservation of momentum, we show both analytically and numerically that the photon-phonon interaction within the resonator cavity causes a moving train of electrodes - a virtual grating of matter density – that displace material in different directions and magnitudes. This hyper-acoustic mode leads to the formation of a high-order Stokes optical line where the sum of the momentum between the Stokes line and the Surface Acoustic Wave is equal to that of the pump optical mode. We calculate three distinct families of SAW – longitudinal, transverse, and Rayleigh-type, and leave open the possibility of sub-families or other deformation types, such as Love waves. Finally, we perform spectroscopy on these SAW and find that high-order modes exist, we calculate their structure, and find that their velocities match the analyticly predicted bulk rate within 1% at high-order SAW modes.

Keywords: surface acoustic waves, SAW, microresonator, Stokes.

1. Introduction

Since the time of Rayleigh, we have understood that surface acoustics may resonate much further than several wavelengths, and in the case of whispering galleries [1] the acoustic waves may circulate in a resonator many times, relative to the acoustic quality factor. Rayleigh used his observations to describe vibrational phenomena on elastic solids, particularly seismic waves resultant from earthquakes [2]. Over the last century, researchers have extrapolated Rayleigh's work to include all manner of acoustic (mechanical) waves propagating across elastic solids, even solids considered extremely rigid. This research benefited a wide variety of fields including sensors, seismology, vehicle engineering, and aeronautic/astronomic engineering.

Beginning in the early 2000s, researchers have considered the opto-mechanical interaction within optical whispering gallery resonators (WGR). The vectors of interaction include optical pressure [3], gradient force [4,5, and electrostriction [6]. This work describes the use of electrostriction in the forward-scattered regime unlike previous work which examined it in the Brillouin backscattered direction [6, 7, 8]. Electrostriction results from the interaction between two optical WGR modes in ultra-high Q cavities, creating a virtual train of regions of high (maxima) and low (minima) density with nodes between. This train of maxima acts as a grating which then serves to maintain the process of scattering a Stokes field from the pump light, thereby is established a self-consistent system.

1.1 Experimental Setup

In this work, we calculate a wide variety of optical modes, find points of level-crossing [9], and analyze the resultant SAW. As a brief introduction to our graphics, Fig 1 illustrates how we refer to calculations of our modes. Both optical [6] and acoustic [8] resonances can be illustrated in this manner. We illustrate by way of cross-sections, either from the 'side' XY plane (assuming the equator lay at Y=0), or from the 'top' XZ plane. We generally present deformed images, where the deformation is proportional to the actual deformation caused by the optical or acoustic mode.

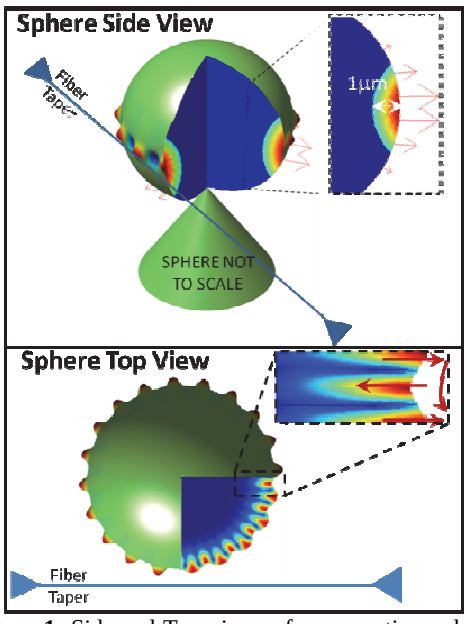

Figure 1: Side and Top views of an acoustic mode in a WGR. We present cross sectional images of the optical and acoustic modes with arrows indicating the direction of material displacement (mode direction of travel). The Side View image shows an undeformed plot of a first order M=20 Rayleigh-type SAW mode on the XY plane (tilted for clarity), and the Top View image shows a deformed plot of a first-order M=20 Rayleigh-type SAW mode on the XZ plane.

2. Optical Modes

We calculate the first 60 states of each optical mode, M, from M=200 to M=764 using Oxborrow's method for calculating optical modes in an axisymmetric dielectric WGR [10,11] as a guide, and modified his technique to calculate spheres. Optical mode refers to the number of optical wave maxima circumferentially along the equator of the microresonator. By calculating via mode we are able to extrapolate linearly to determine the wavelength, , of a given frequency of optical wave in a WGR of known radius. We have found through calculations that the mode versus frequency values vary linearly according to the formula

$$\lambda = \frac{2\pi r}{M}.$$

For example, in a radius r=75 micron spherical silica WGR by input wavelengths of 617 nanometers results in M=764 while an input optical of 2.4 micron corresponds to M=200. Our data predicts optical interaction between optical modes to produce a corresponding acoustic mode from visible to far IR light. We can vary the radius within microsphere ranges (50 to 150 microns) and use this dataset effectively to determine the optical modes inducing a SAW of given frequency. Furthermore, we can expand this table as needed by running further calculations.

2.1 Optical States

Interestingly, an optical mode may have a variety of states, as mentioned above. These states manifest in the WGR with the same azimuthal M and wavelength, but may have more than a single maxima in the transverse directions. Using the mode index *M=(l, m, n)* where $1 \leq (l, m, n)$ and *l* represents the number of maxima in the azimuthial direction (east-west along equator), *m* represents the number in the polar direction (north-south centered on equator), and *n* represents the radial direction (in-out terminating at the surface, centered at the equator) we will see a wide variety of spectral activity in the optical domain. For example, M=(618,1,1) is the first state of mode 618 and has a wavelength of 1.50 micron and the expected frequency of 278.119THz in a radius 75 micron microsphere WGR. In the same sphere, M=(606,1,2) is the 13th state of mode 604 with a wavelength of 1.100 microns and a frequency of 278.066THz while M=(606,13,1) is the 14th state of mode 604 with wavelength 1.100 microns and a frequency of 278.130THz.

2.2 Optical Mode Interaction

Taking M=(618,1,1) as the first optical mode, we see that we can use the transition between M=(606,1,2) and M=(606,13,1) as the point of optical interaction to produce the M=12 SAW, as acoustic azimuthal mode number is simply the difference between the azimuthal mode numbers of the interacting optical modes. Fig. 2 illustrates these two optical modes interacting to produce an acoustic wave of M=12. Note that once crossing occurs, it continues as frequency increases; this is true in general – when $\Delta M = M_{opt1} - M_{opt2}$, two modes separated azimuthally by M will cross at state M+1 with many subsequent crossings.

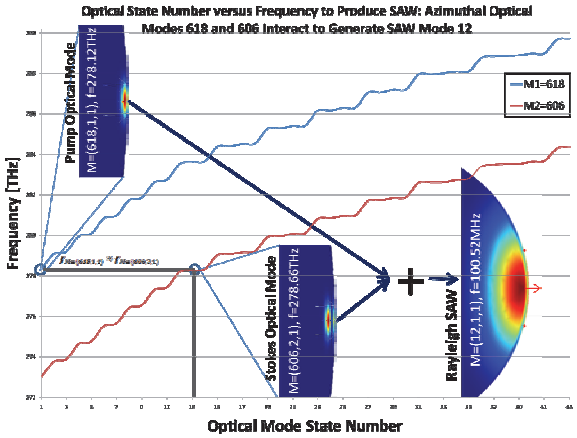

Figure 2: Calculated optical states versus frequency. Two optical modes will cross within ΔM azimuthal modes and ΔM +1 mode states. Here the optical modes are separated by ΔM =12 and are depicted to produce an M=(12,1,1) Rayleigh-type SAW, however any M=(12,m,n) SAW mode is possible.

2.3. SAW Velocities

In [8] we presented four distinct families of SAW in the backward-scattered direction– longitudinal, transverse polar, transverse radial, and Rayleigh type. Here, we present three of those families – longitudinal, transverse polar, and Rayleigh-type – in the forward scattered direction. As in that work, SAW wave velocity is tied to the acoustic azimuthal mode number – as the number increases, the wave interacts with the WGR material more. This interaction results in a slowing of the wave. State of the wave is important, as higher states interact with differing portions of the material – and as such have a higher frequency and velocity than the base M=(*l*,1,1) mode. Also like the back-scattered case, as M azimuthal increases, the velocity of a given wave family approaches the analytic solution of that wave family on a planar solid-air boundary. Table 1 is copied in part from [8] in order to show the analytic solutions of the velocity of each wave family in bulk.

We calculated each of these three families using the methods developed by [6] and modified by [8], however in this instance we were not limited by the acoustic wavelength set at one half the pump optical wavelength as in the back-scattered case [3], rather the acoustic wavelength can be any such that the following equations are satisfied:

$$M_{o1} - M_{o2} = \mathrm{M}_{\mathrm{SAW}}, \quad f_{o1} - f_{o2} \approx f_{saw},$$
and $k_{pump} = k_{Stokes} + k_{SAW}$

We calculated many azimuthal mode velocities in the range M=10 through M=2000. We present in Fig 3 our findings of the first three states of Rayleigh-type SAWs. Figure 4 shows each of our analyzed wave families velocities versus mode number. For ease of reading we have limited the mode number in the figures; our full data show continuance towards convergence with the analytically calculated and experimentally shown velocity [13-16] in planar bulk media. We note that in every instance, the mode family converges toward the analytic planar SiO_2-air SAW velocity solution. In our calculations, we solved for frequency versus mode number. Here we present velocity versus mode number to illustrate the convergence using the following well-known conversion:

$$v_i = \frac{2\pi r f}{M}.$$

Table 1: Analytic SAW Velocities in SiO_2 [8,9,10]
V_i family *i* velocity, *E* elasticity, density, Poisson ratio

Wave	Velocity [m/s]
Longitudinal	$V_L = \sqrt{\frac{E(1-\nu)}{\rho(2\nu^2+\nu-1)}} = 5040$
Shear	$V_S = \sqrt{\frac{E}{2\rho(\nu+1)}} = 3637$
Rayleigh	$V_R = \frac{V_S(0.87+1.12\nu)}{(1+\nu)} = 3410$

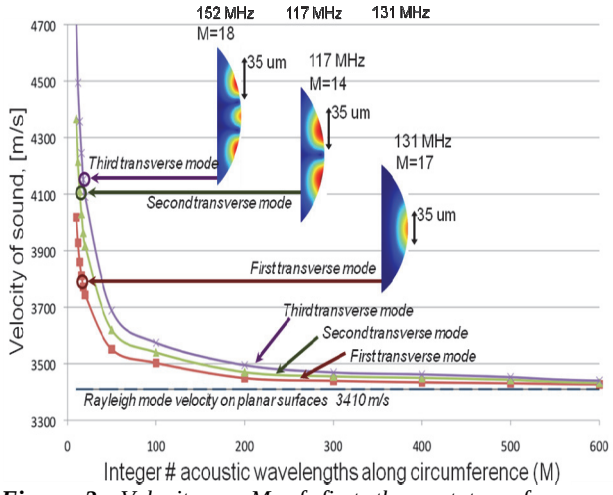

Figure 3: *Velocity vs M of first three states of Rayleigh-type waves (inset) from M=10 to M=600. As the M increases, the velocities of the acoustic waves converge towards the analytic solution.*

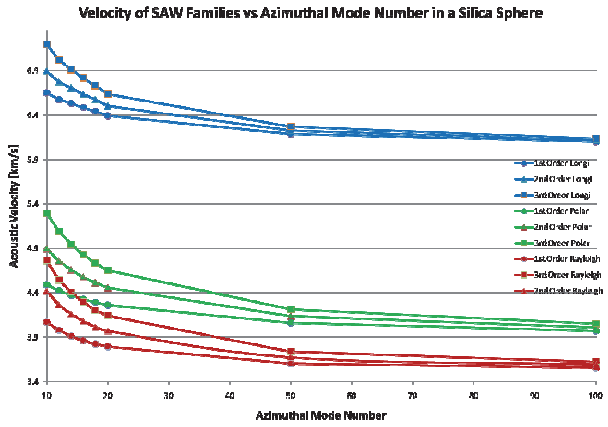

Figure 4: Velocity of three SAW families vs mode number. All three families converge towards the analytic planar solution as mode number increases. The term 'order' represents the number of maxima along the polar direction, as in figure 12, above. Note the crossing between transverse polar M=(15,1,1) and Rayleigh M=(15,1,3).

3. Use of COMSOL Multiphysics

As described in Table 1, we sought to find appropriate Surface Acoustic Modes describing the analyticaly predicted and experimentally found velocities. In order to do this, we first had to devise a method by which we would obtain the finest mesh while retaining the authentic structure of the microsphere in a 3D stress-strain eigenfrequency simulation. We found that we could calculate slices of single wavelengths, or portions of single wavelengths in the azimuthal direction. We also found that SAWs have a compact waveform and thus need only limited real-estate in the polar and radial directions. In order to capture higher-order modes, we retained five wavelengths of material in the polar direction and two wavelengths in the radial. We, therefore, took a piece of a sphere with the following dimensions: $<2\lambda,0.25\lambda,5\lambda>$ in polar coordinates. Built this section first in 2D, then cast it into 3D in four layers.

Next, we used our boundary conditions (BC) to isolate the particular waveforms. We note that modification of BC is *not* essential, but given limited RAM and time, we set BC in order to more efficiently sift out the desired solutions.

For longitudinal modes, we held one outside slice Fixed and set the opposite slice to Anti-Symmetry Plane. For transverse (both families), we held one outside slice Fixed and the other as a Symmetry Plane. Generally, these BC settings find the first 60 transverse and longitudinal mode states with very few 'noise' states.

Rayleigh-type wave simulation requires a different approach. Here we must calculate half or full wavelength slices, or else the solution appears as a transverse radial. The BCs are Symmetry Plane and Symmetry Plane on the outside. Rayleigh-type waves only occur at the surface, so COMSOL (at a medium-grade mesh) will find far fewer of these modes and inject a lot more 'noise.' We have found as many as 10 maxima in the polar direction by using longer slices.

To calculate the optical modes discussed in section 2.1, we simply wrote a Matlab script to repeatedly run the Oxborrow COMSOL file [11] to find 60 states per optical mode for modes M=200 to M=950, saving figure files and adding frequency information to a CSV file for each state. This process took, on average, 6 minutes per state, but resulted in excellent data and a very extensive library of optical mode figures and frequencies.

4. Conclusion

Here we presented the theoretical background and calculations to show that Stokes interaction between co-propagating optical waves can and do produce SAWs. The co-propagating optical waves cross at a predictable

interval and tend to follow the pattern of the previous wave.

The forward-scattered SAWs are not constrained by conservation of momentum to have twice a momentum vector twice the magnitude of the pump optical wave's momentum vector, but may instead have any momentum vector magnitude so long as $k_{pump} = k_{Stokes} + k_{SAW}$ holds. These SAW modes may come in any of the three primary families as their backward-scattered cousins: longitudinal, transverse, and Rayleigh-type. These SAWs may also have many maxima in the azimuthal, radial, and polar directions.

Forward-scattered waves may benefit several areas of interest including: local oscillators, machine olfactorization, signaling, and other sensor applications.

8. References

Type your references here, as needed.

1. L. Rayleigh, *Philos. Mag* 20 (1910) 1001.
2. L. Rayleigh, *Proceedings of the London Mathematical Society* 1 (1885) 4.
3. T. Carmon, H. Rokhsari, L. Yang, T. J. Kippenberg, and K. J. Vahala, *Physical Review Letters* 94 (2005) 223902.
4. Q. Lin, X. Jiang, M. Eichenfield, R. Camacho, P. Herring, K. Vahala, and O. Painter, in *Conference on Lasers and Electro-Optics/International Quantum Electronics Conference 2009*, OSA, Baltimore, Maryland, 2009, p. CMKK1.
5. X. Jiang, Q. Lin, J. Rosenberg, K. Vahala, and O. Painter, Optics Express 17 (2009) 20911.
6. M. Tomes and T. Carmon, *Physical Review Letters* 102 (2009) 113601.
7. A. B. Matsko, A. A. Savchenkov, V. S. Ilchenko, D. Seidel, and L. Maleki, *Physical Review Letters* 103 (2009) 257403.
8. J. Zehnpfennig, M. Tomes, and T. Carmon, in *2010 International Conference on Optical MEMS and Nanophotonics (OPT MEMS)*, IEEE, Sapparo, Japan, 2010, p. 51.
9. T. Carmon, H. G. L. Schwefel, L. Yang, M. Oxborrow, A. D. Stone, and K. J. Vahala, *Physical Review Letters* 100 (2008) 103905.
10. M. Oxborrow, in *Laser Resonators and Beam Control* IX, Vol. 6452 (A. V. Kudryashov, A. H. Paxton, and V. S. Ilchenko, eds.), SPIE, 2007.
11. M. Oxborrow, in 2.5-D Simulation of Axi-Symmetric Electromagnetic Structures via Weak Forms, 2003.
12. R. W. Boyd, *Nonlinear Optics*, Chapter 9, Academic Press, Amsterdam ; Boston, 2008.
13. Pham Chi Vinh and P. G. Malischewsky, *Journal of Thermoplastic Composite Materials* 21 (2008) 337.
15 T. Carmon, University of Michigan, Ann Arbor, MI, 2009.
16. L. Kinsler, A. Frey, A. Coppens, and J. Sanders, *Fundamentals of acoustics*, 3 ed. (John Wiley & Sons, Inc, 1999).
17. D. S. Ballantine and Knovel, *Acoustic wave sensors: theory, design, and physico-chemical applications*, Academic Press, San Diego, 1997.